ACS APPLIED MATERIALS & INTERFACES

Research Article

www.acsami.org

One-Step Chemical Synthesis of ZnO/Graphene Oxide Molecular Hybrids for High-Temperature Thermoelectric Applications

Dongsheng Chen,[†,⊥] Yan Zhao,[†,‡] Yani Chen,[†] Biao Wang,[§] Haiyan Chen,[‡] Jun Zhou,[§] and Ziqi Liang*[,†]

[†]Department of Materials Science, Fudan University, Shanghai 200433, China

[‡]Shanghai Advanced Research Institute, Chinese Academy of Sciences, Shanghai 201210, China

[§]Center for Phononics and Thermal Energy Science, School of Physics Science and Engineering, Tongji University, Shanghai 200092, China

[⊥]College of Mathematics and Physics, Shanghai University of Electric Power, Shanghai 200090, China

Supporting Information

ABSTRACT: ZnO as high-temperature thermoelectric material suffers from high lattice thermal conductivity and poor electrical conductivity. Al is often used to n-dope ZnO to form $Zn_{1-x}Al_xO$ (AZO). Owing to very limited Al solubility (less than 2 atom %) in AZO, however, electrical conductivity is difficult to improve further. Moreover, such a low concentration of Al dopants can hardly reduce the thermal conductivity. Here, we propose slightly adding chemically reduced graphene oxides (rGOs) to AZO in various contents to modulate the carrier concentration and simultaneously optimize the electrical and thermal conductivities. Such nanocomposites with rGO embedded in AZO matrix are formed on the molecular level by one-step solution chemistry method. No obvious changes are found in crystalline structures of AZO after introducing rGOs. The rGO inclusions are shown to uniformly mix the AZO matrix that consists of compacted nanoparticles. In such AZO/rGO hybrids, Zn^{2+} is captured by the rGO, releasing extra electrons and thus increasing electron density, as confirmed by Hall measurements. The phonon-boundary scattering at the interface between AZO and rGO remarkably reduces the lattice thermal conductivity. Therefore, a respectable thermoelectric figure of merit of 0.28 at 900 °C is obtained in these nanocomposites at the rGO content of 1.5 wt %, which is 8 times larger than that of pure ZnO and 60% larger than that of alloyed AZO. This work demonstrates a facile wet chemistry route to produce nanostructured thermoelectric composites in which electrical conductivity can be greatly increased while largely lowering thermal conductivity, collectively enhancing the thermoelectric performance.

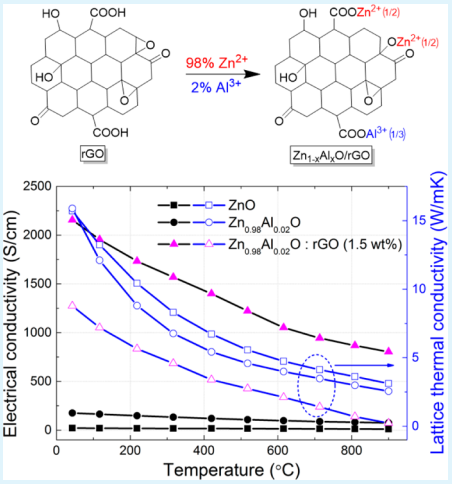

KEYWORDS: *Al-doped ZnO, reduced graphene oxide, hybrids/nanocomposites, solution processing, thermoelectric materials*

1. INTRODUCTION

Thermoelectric (TE) materials can directly transfer waste heat from automobile exhaust systems or excess solar thermal flux into electrical power.[1,2] These energy utilizations are eco-friendly and non-polluting. Therefore, TE devices have been recognized for a long time as a highly promising transformative technology to reduce global energy consumption. Research on TE materials has attracted great interest from both scientific and industrial communities.[3−6] The TE performance is characterized by a dimensionless figure of merit $zT = S^2\sigma T/\kappa$, where T is the absolute temperature, S is the Seebeck coefficient, σ is the electrical conductivity, and κ is the thermal conductivity which consists of the electronic thermal conductivity (κ_e) and the lattice thermal conductivity (κ_L). Therefore, the simultaneous increase of electrical conductivity and Seebeck coefficient along with reduction of thermal conductivity are favorable for the enhancement of zT.

By far, the most efficient TE materials include $Bi_{2-x}Sb_xTe_3$-based materials near room temperature,[7] PbTe-based materials in medium temperature regime (500−900 K),[8] and SiGe alloys in high temperature regime (>900 K).[9,10] All these materials contain elements such as Bi, Pb, Te, and Ge, which are expensive and toxic. Recently, ZnO became a potential candidate for high-temperature TE materials due to its nontoxicity, low cost, and excellent thermal stability.[11] However, the main drawback of ZnO for TE applications is its low electrical conductivity due to the low carrier concentration. Adding dopants is considered a feasible route to increasing the carrier concentration. For example, Al and Ga were often used n-type dopants for ZnO while tuning its crystal structure due to the similar ionic radii of Al^{3+} and Ga^{3+} to that

Received: November 11, 2014
Accepted: January 21, 2015
Published: January 21, 2015

DOI: 10.1021/am507882f
ACS Appl. Mater. Interfaces 2015, 7, 3224−3230

Figure 1. Schematic of the experimental procedure for preparing AZO/rGO hybrid materials.

of Zn^{2+}.[12] These doped ZnO-based oxides—Al-doped ZnO (AZO), Ga-doped ZnO (GZO), and Al and Ga codoped ZnO—have been successfully made for realization of high temperature TE power generation.[13−17] For instance, AZO with an optimum composition ratio, $Zn_{0.98}Al_{0.02}O$, reached a high zT of 0.30 at 1000 °C by ball-milling Al_2O_3 and ZnO powders.[15] Al and Ga codoped ZnO with an optimum composition ratio, $Zn_{0.98}Al_{0.02}Ga_{0.02}O$, reached a high zT of 0.65 at 1000 K by sintering a mixed powder of ZnO, Al_2O_3, and Ga_2O_3. More recently, a zT of 0.44 at 1000 K was obtained in AZO that was made by microwave synthesis with an average size of ∼65 nm.[16] However, the miscibility of Al (or Ga) with ZnO was very poor. Moreover, excessive Al (or Ga) contents inevitably resulted in a secondary phase, which would deteriorate carrier transport properties.[12] An alternatively effective approach is thus highly needed for creating doped ZnO nanocomposites to ensure the molecular miscibility while enhancing the electrical conductivity.

The formation of organic−inorganic hybrids with doped material can not only increase the carrier concentration but also reduce the thermal conductivity due to phonon-boundary scattering at interfaces, thereby greatly improving the TE performance.[18−20] For instance, $Zn_{1-x}Ni_xO$/polyparaphenylene (PPP) composites were shown to optimize the TE performance with simultaneous electrical conductivity enhancement and thermal conductivity reduction.[21] The hybrid materials exhibited dual effects of both increasing electrical conductivity and reducing thermal conductivity. Optimum $Zn_{0.95}Ni_{0.05}O$/PPP nanocomposites containing 5 wt % PPP exhibited an increase of electrical conductivity by ∼45% at 650 K and a reduction of thermal conductivity by ∼30% at 1173 K. On the other hand, graphene, a two-dimensional (2D) flat monolayer of sp^2-bonded carbon atoms, has recently attracted tremendous attention owing to its superior merits of large specific surface area and good electrical conductivity.[22] These favorable characteristics make graphenes potentially excellent TE materials.[23−25] Therefore, it can be envisioned that integration of graphene into inorganic TE materials would enhance their TE performance. One such example was recently reported by Dong et al. that the in situ chemistry method was used for PbTe−graphene nanocomposites for TE applications.[26] In their work, PbTe nanoparticles were uniformly anchored on the surface of graphene which was used as both the dispersant and the 2D growth template, forming a unique hybrid nanostructure. The ultrahigh electron mobility of graphene improved the electrical conductivity of the nanocomposites, while the intercalative hybrid structures increased the concentration of interfaces which resulted in the greatly lowered thermal conductivity.

To our knowledge, there are few reports on utilizing graphene to enhance the TE properties of ZnO. Here, we report a wet chemistry method of in situ preparation of bulk composite materials of AZO and reduced graphene oxide (rGO) for TE applications. Solution fabrication of hybrid materials enables the formation of nanostructured composites on the molecular level and the use of facile doping methods to enhance the TE properties.[27] Compared to pure AZO, the slightly graphene doped nanocomposites in this study can significantly improve TE properties of AZO with an increase of electrical conductivity and a reduction of thermal conductivity. We obtained a maximum zT value of 0.28 at 900 °C, which is 8 times larger than that of pure ZnO and 60% larger than that of alloyed AZO. In such AZO/rGO nanocomposites, the introduction of rGO offers a novel way to modulate the carrier concentration which is crucial of improving the TE properties. During the preparation of this report, the latest report by Lee et al. demonstrated the similar preparation of single-crystalline ZnO−rGO nanocomposites; however they were made using a two-step wet chemistry method.[28]

2. RESULTS AND DISCUSSION

2.1. Synthesis of AZO/rGO Nanocomposites. A facile one-step method of chemical synthesis was used to fabricate molecular hybrid materials of AZO/rGO. The experimental procedure is schematically illustrated in Figure 1, and the details are described in the Experimental Section. Two batches of precursor solutions—rGO and a mixture of $Zn(NO_3)_2·6H_2O$ and $Al(NO_3)_3·9H_2O$ (1−2 atom %) in deionized water—were prepared and then mixed overnight at room temperature. After the mixture was heated to 100 °C, a viscous gel formed and was dried overnight at 80 °C under vacuum. The crude products were ground into fine powders and then subject to vacuum annealing at 500 °C for 2 h, forming the AZO/rGO hybrids. For simplicity of discussion and also because of better electrical conductivity in 2 atom % Al-doped ZnO, we chose $Zn_{0.98}Al_{0.02}O$/rGO hybrids for the following comparative studies in which ZnO and AZO ($Zn_{0.99}Al_{0.01}O$ and $Zn_{0.98}Al_{0.02}O$) nanoparticles were prepared separately.

As schematically depicted in Figure 2, the hybrid composite $Zn_{0.98}Al_{0.02}O$/rGO, for instance, was formed by adsorption of Zn^{2+} (majority, 98 atom %) and Al^{3+} (minority, 1−2 atom %) ions onto the surface of the rGO nanosheets, and their subsequent chemical reactions with carboxylic acid, hydroxyl,

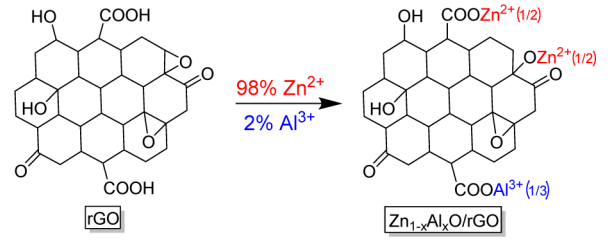

Figure 2. Schematic illustration of possible mechanisms of forming the $Zn_{0.98}Al_{0.02}O$/rGO composites as an example.

DOI: 10.1021/am507882f
ACS Appl. Mater. Interfaces 2015, 7, 3224−3230

and carbonyl groups of rGOs. During the hybrid formation, both Zn^{2+} and Al^{3+} ions were captured by rGO, thus releasing extra electrons and increasing electron carrier concentration. Thus, introduction of rGOs to AZO is expected to enhance the TE performance.

2.2. Phase Structures. X-ray diffraction (XRD) experiments were conducted for studying the influences of Al-doping and rGO addition on the crystalline structures of ZnO, and the comparative results are shown in Figure 3. The pure ZnO sample displayed all characteristic orientation peaks as marked in the figure. Upon the addition of Al at 1 atom % and 2 atom %, respectively, the alloyed $Zn_{1-x}Al_xO$ samples showed no difference of XRD patterns from pure ZnO, indicating that delicate Al-doping did not change the crystalline structures of ZnO. Furthermore, when introducing rGO at various contents of 1.5, 2.5, and 3.5 wt % to form the AZO/rGO nanocomposites, the XRD patterns remained nearly the same, also implying the little influence of rGO on the crystalline structures of ZnO.

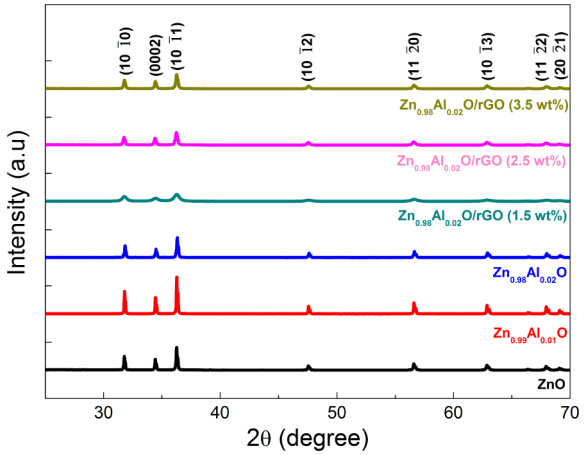

Figure 3. XRD patterns of AZO/rGO nanocomposites in comparison with ZnO and AZO.

2.3. Morphology. Figure 4 displays the morphologies of the pure ZnO, AZO alloys, and $Zn_{0.98}Al_{0.02}O$/rGO hybrids, as measured by field-effect scanning electron microscopy (FE-SEM). Note that these SEM images mainly visualize ZnO particles, as well as slight Al dopants, and the rGO domains are nearly invisible due to the nature of the ultrathin layers. Figure 4a shows the agglomerated and nonuniform ZnO powders with an average size of 200−400 nm. Figure 4b reveals the existence of Al in the composite powders, as marked in red circles and confirmed by energy-dispersive X-ray (EDX) profiles (Figure S1, Supporting Information). As shown in Figure 4c, with increasing Al content, the grain size of the AZO particles became smaller and more agglomerated. Al doping not only restricts the AZO particle size during the synthesis but also inhibits its grain growth during sintering presumably by grain boundary pinning.[16] In the $Zn_{0.98}Al_{0.02}O$/rGO hybrids, however, the AZO particle sizes were smaller and more uniform at a content of 1.5 wt % rGO (Figure 4d) because the presence of rGO was dispersed between AZO particles, which hindered the AZO grain growth. As the rGO content increased to 2.5 wt %, the particle sizes became nonuniform again (Figure 4e) due to the aggregation of rGO nanosheets. Furthermore, at the rGO content of 3.5 wt %, more aggregated rGO nanosheets were difficult to disperse between ZnO particles and as a result the particle sizes became bigger (Figure 4f).

2.4. Hall Measurements. We performed Hall measurements on the above samples to obtain the Hall mobilities (μ_H) and the carrier concentrations (n_e). Figure 5a shows their dependence on Al contents (atom %), in which n_e increased from 1.22×10^{18} cm^{-3} in pure ZnO to 1.5×10^{19} cm^{-3} and 3.17×10^{19} cm^{-3} in AZO with 1.0 and 2.0 atom % Al contents, respectively. This is due to the substitution of Zn^{2+} with Al^{3+} in AZO, creating one more electron. The μ_H first decreased from 16.7 cm^2 V^{-1} s^{-1} in pure ZnO to 15.9 cm^2 V^{-1} s^{-1} in AZO with 1.0 atom % Al content, owing to the ionized impurity (Al^{3+}) scattering. Then, the μ_H increased to 22.9 cm^2 V^{-1} s^{-1} in the doped sample with 2.0 atom % Al content, possibly due to the distortion of band structures of ZnO by excessive Al doping. The reason is that the μ_H is inversely proportional to the

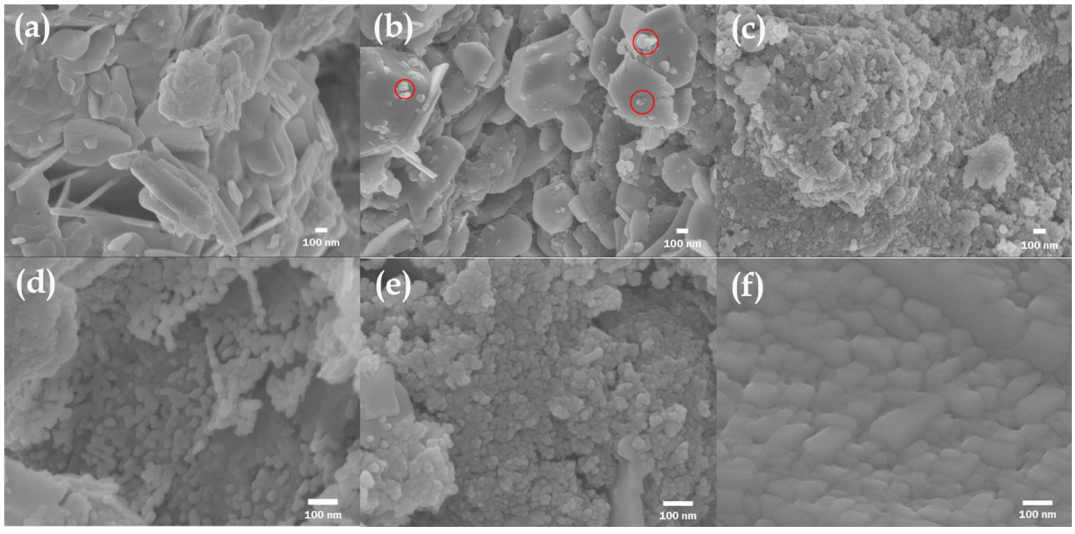

Figure 4. SEM images of (a) ZnO, (b) $Zn_{0.99}Al_{0.01}O$, (c) $Zn_{0.98}Al_{0.02}O$, (d) $Zn_{0.98}Al_{0.02}O$/rGO (1.5 wt %), (e) $Zn_{0.98}Al_{0.02}O$/rGO (2.5 wt %), and (f) $Zn_{0.98}Al_{0.02}O$/rGO (3.5 wt %). Red circles indicate the Al in AZO as confirmed by EDX measurement.

DOI: 10.1021/am507882f
ACS Appl. Mater. Interfaces 2015, 7, 3224−3230

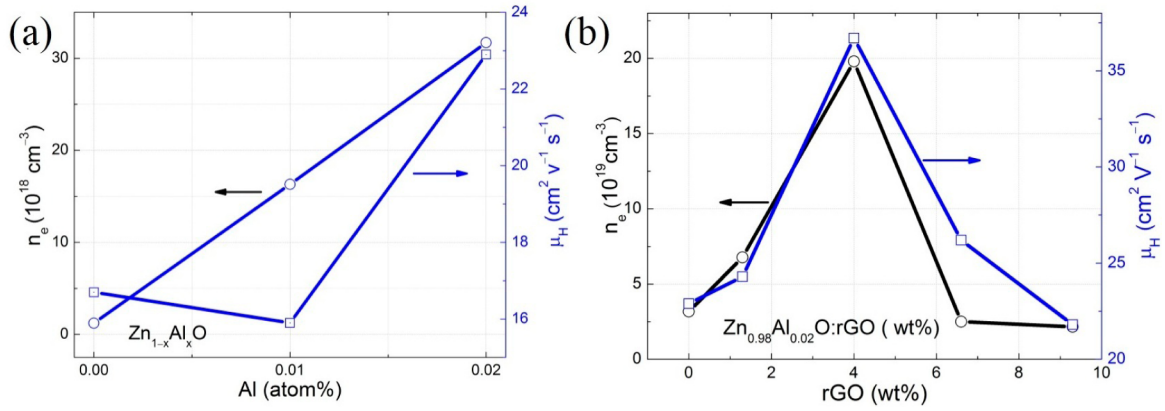

Figure 5. Hall spectra of (a) AZO and (b) AZO/rGO nanocomposites.

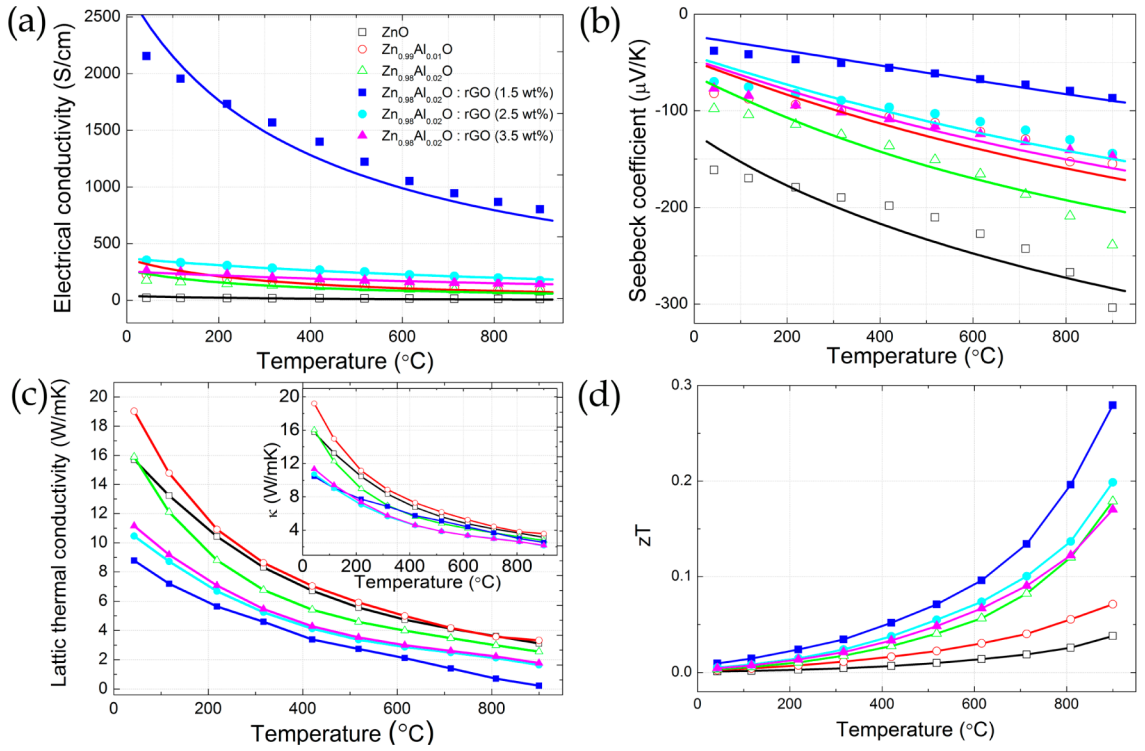

Figure 6. Temperature dependence of TE properties of AZO and AZO/rGO composites in the range of 25−900 °C. (a) Electrical conductivity; (b) Seebeck coefficient; (c) lattice thermal conductivity, (inset) total thermal conductivity (κ); and (d) zT. In graphs a and b, the points are experimental data, and the fitted lines are the corresponding simulated results. In graphs c and d, the lines are plotted as a guide for the eye.

effective mass, which is an important parameter of band structure and can be changed when Al is doped into ZnO.

When introducing rGO into AZO, both n_e and μ_H increased first and then decreased as the rGO content increased (Figure 5b). The maximum n_e (1.98×10^{20} cm^{-3}) and μ_H were reached at the rGO content of 1.5 wt %. To explain such variations that depend strongly on the rGO contents, we propose that there exist two competing mechanisms that affect the n_e. On one hand, the majority of Zn^{2+} ions are captured by rGO to release extra electrons, causing a significant increase of n_e.[26] In other words, the carbons in rGO act as the donor in the ZnO crystal lattice.[28] On the other hand, rGO acts as a p-type dopant in AZO, which would decrease n_e. As seen from Figure 5b, when the content of rGO was smaller than 1.5 wt %, the dependence of rGO content was dominated by the former mechanism, while the latter mechanism accounted for that of rGO contents greater than 1.5 wt %. Similar experimental results were recently reported on PbTe−graphene nanocomposites;[26] however, researchers failed to interpret the slight decrease of carrier density when the rGO content was higher than the optimum 10 wt %. As for μ_H, there are the same tendency as n_e in Figure 5b. Considerably high electron mobility of graphene accounts for such a tendency when the rGO content is smaller than 1.5 wt %. However, higher rGO content (2.5 and 3.5 wt %) can result in much more interface concentrations between $Zn_{1-x}Al_xO$ and rGO, which cause the reduction of μ_H value.

2.5. Thermoelectric Properties. The electrical conductivity and the Seebeck coefficient were measured simultaneously by the steady-state four-probe method in the range of temperature of 25−900 °C. The experimental results of electrical conductivity and Seebeck coefficient were fitted by using the following Boltzmann transport equations:[29]

DOI: 10.1021/am507882f
ACS Appl. Mater. Interfaces 2015, 7, 3224−3230

$$\sigma = \frac{e^2}{3\pi^2 m^*}\int k^3\tau(E)\left(\frac{\partial f_0}{\partial E}\right)\mathrm{d}E \quad (1a)$$

$$S = \frac{1}{eT}\frac{\int k^3\tau(E)(E-\mu)\left(-\frac{\partial f_0}{\partial E}\right)\mathrm{d}E}{\int k^3\tau(E)\left(-\frac{\partial f_0}{\partial E}\right)\mathrm{d}E} \quad (1b)$$

where e is the electron charge; m^* is the effective mass of electron; k is the wave vector of electron; μ is the chemical potential; $E = \hbar^2k^2/(2m^*)$ is the kinetic energy of electron, where $\hbar$ is the Plank constant; and $f_0 = \{\exp[(E-\mu)/(k_BT)]+1\}^{-1}$ is the Fermi–Dirac distribution, where k_B is the Boltzmann constant. The energy dependent relaxation time τ is calculated by using the Mathiessien's rule.[30] All the possible scattering mechanisms such as the electron-acoustic phonon scattering, the electron–optical phonon scattering, the electron-impurity scattering, and the electron–interface scatterings were considered in our calculations.[31,32]

Figure 6a shows the temperature dependence of electrical conductivity of AZO/rGO nanocomposites. The points are the experimental data, and the curves with the same color are the theoretical fitting with reasonable fitting parameters. The calculated results are in good agreement with the experimental data. We found that the σ decreased gradually with increasing temperature since the relaxation time of the electron–phonon scattering in eq 1a is inversely proportional to the temperature. As for different samples at room temperature, σ increased from 21.6 S/cm in pure ZnO to 176 S/cm in AZO with 2.0 atom % Al content. Furthermore, in the $Zn_{0.98}Al_{0.02}O$/rGO sample, σ was greatly enhanced. When the content of rGO was 1.5 wt %, σ attained the maximum value of 2200 S/cm at room temperature, which is 10 times larger than that of $Zn_{0.98}Al_{0.02}O$ due to the highest carrier concentration of AZO/r-GO hybrids. Although σ then decreased to 1000 S/cm at 900 °C, it still remained much higher than that in all of the other samples. As the rGO content increased to 2.5 and 3.5 wt %, σ further decreased because of lower carrier concentration as indicated in Figure 5b.

Figure 6b shows the temperature dependence of the Seebeck coefficient (S) of AZO/rGO nanocomposites in comparison with pure ZnO and alloyed AZO. The sign of S is always negative for all samples, indicating that the charge carriers are electrons rather than holes. The absolute value of S monotonically increased with increasing temperature since more electrons are distributed to high energy states; in other words, the average energy of electrons becomes larger. The absolute value of S first decreased and then increased with increasing Al contents. The absolute S in the AZO/rGO hybrids with 1.5 wt % rGO content was lower than that in AZO. Further increasing the rGO content (>1.5 wt %), the carrier concentration was significantly decreased and thus the absolute S increased yet not exceeding that of AZO.

Figure 6c shows the temperature dependence of the lattice thermal conductivity (κ_L) of all samples with an inset showing the dependence of total thermal conductivity (κ). The κ_L ($= \kappa - \kappa_e$) was calculated using the Wiedemann–Franz law $\kappa_e = L\sigma T$, where L is Lorentz number (2.45×10^{-8} W Ω K^{-2}).[1,2] With increasing temperature, both κ and κ_L were reduced due to stronger phonon–phonon scattering. With increasing Al content from 1 atom % to 2 atom %, both κ and κ_L decreased because of additional phonon-impurity scattering where Al atoms play rules as scattering centers. When the rGO was introduced to the $Zn_{0.98}Al_{0.02}O$, κ_L increased with increasing rGO content. κ_L is affected collectively by increased thermal conductivity with increasing rGO content, and decreased thermal conductivity resulting from the phonon–boundary scattering between AZO and rGO.[33] By contrast, the variation of κ with the rGO content (Figure 6c inset) is more complicated because κ is the sum of $L\sigma T$ and κ_L where σ decreased with increasing rGO content (Figure 6a), while κ_L increased as discussed above. As a result, the lowest κ_L was reached at 900 °C for the sample with the lowest 1.5 wt % rGO content, while the lowest κ was reached for the sample with the highest 3.5 wt % rGO content.

As a consequence, the zT values of all the samples are calculated and shown in Figure 6d. The highest zT of 0.28 was obtained at 900 °C in $Zn_{0.98}Al_{0.02}O$/rGO (1.5 wt %), 8 times larger than that of pure ZnO sample and 60% larger than that of the $Zn_{0.98}Al_{0.02}O$ sample. This indicates that integration of rGO into ZnO to generate the molecular hybrids is a promising approach to a significant increase of electrical conductivity while considerably lowering the lattice thermal conductivity, collectively leading to a respectable zT.

It should be noted that low zT values of AZO/rGO hybrids primarily resulted from the poor TE performance of as-synthesized AZO, which is nevertheless consistent with the previous results by others.[13,21] The reason is that the much larger size of AZO domains produced in this method, as compared to those produced by microwave synthesis,[16] is difficult to reduce the thermal conductivity.[33] Future work will thus focus on developing an improved synthetic route to AZO nanoparticles with highly reduced size, which will lead to significantly improved TE performance of AZO and its hybrids with rGO.

3. CONCLUSIONS

In summary, we have demonstrated a one-step solution chemistry route to create molecular-level nanostructured thermoelectric composites of AZO/rGO. Introduction of rGOs into AZO remarkably increases the carrier concentration and creates more domain boundaries, resulting in higher electrical conductivity and lower thermal conductivity. Effects of rGO contents on the thermoelectric properties of AZO based nanocomposites have been investigated. The maximum zT value of about 0.28 was obtained at 900 °C for the nanocomposites with the 1.5 wt % rGO content, 8 times and 60% higher than that of pure ZnO and AZO, respectively. It is envisioned that further increasing zT requires the significantly lower thermal conductivity, which can be achieved by introducing the heavy atom into the molecular hybrids.

4. EXPERIMENTAL SECTION

4.1. Preparation of ZnO–Graphene Oxide Hybrid Materials.

Two batches of precursor solutions were prepared at first. In one batch, graphite oxides that were prepared from graphite powder (<45 μm, ≥99.99%, Sigma-Aldrich) by a modified Hummer's method were dissolved in 100 mL of deionized water with sonication for 120 min to form a homogeneous solution. To the graphite oxide solution was added 70 μL N_2H_4, and the mixture was heated to 100 °C for 12 h under stirring and reflux to obtain reduced graphene oxides. In the other batch, $Zn(NO_3)_2{\cdot}6H_2O$ (Sinopharm, 98%) was mixed with $Al(NO_3)_3{\cdot}9H_2O$ (Sinopharm, 98%) at 1–2 atom % in 100 mL of deionized water with sonication for 10 min to form a homogeneous mixed solution, followed by aging for 12 h. These two batches of precursors in aqueous solution were then mixed under stirring conditions overnight at room temperature and subsequently heated to

DOI: 10.1021/am507882f
ACS Appl. Mater. Interfaces 2015, 7, 3224–3230

100 °C, forming a viscous gel. The gel was dried overnight at 80 °C under vacuum. The crude products were ground into fine powders and then loaded into a porcelain boat and placed in a vacuum annealing furnace (GSL-1400X, KJMT, Inc., China). The crystalline phases were obtained by calcination of the amorphous xerogel at 500 °C for 2 h, thus forming AZO/rGO nanocomposites. Then, the powders were pressed into circular pellets and sintered at 900 °C and under 75 MPa for 2 h in an Ar atmosphere. For comparison, we made ZnO and AZO nanoparticles according to the method of preparing the second batch of precursor solution.

4.2. Characterizations and Measurements. Phase structures of as-prepared samples were characterized by X-ray diffraction (XRD; Bruker AX D8 Advance) using nickel filtered Cu Kα radiation (λ = 1.5406 Å). XRD pattern data for 2θ values ranging from 25−75° were collected. Field-effect scanning electron microscopy (FE-SEM, Hitachi S-520) coupled with energy-dispersive X-ray (EDX, 20 kV) were used to study the microstructure of the samples. The Hall coefficient measurements were performed on Accent HL5500PC system at room temperature. For thermoelectric measurements, samples were cut into rectangular shapes. The electrical conductivity and Seebeck coefficient were measured simultaneously by the standard four-probe method (Linseis LSR-3/1100) from 25 to 900 °C under a He atmosphere. The thermal conductivity was determined using the equation $\kappa = DC_pd$. The thermal diffusivity (D) was measured using a laser flash apparatus (Linseis LFA 1000), the specific heat (C_p) measurement was conducted on a DSC Q2000 TA differential scanning calorimeter, and the density (d) was determined by the Archimedes' method.

■ ASSOCIATED CONTENT

Ⓢ Supporting Information

EDX profile of AZO composite powder. This material is available free of charge via the Internet at http://pubs.acs.org.

■ AUTHOR INFORMATION

Corresponding Author

*E-mail: zqliang@fudan.edu.cn. Tel.: 86-21-65642816.

Notes

The authors declare no competing financial interest.

■ ACKNOWLEDGMENTS

This work is sponsored by Shanghai Pujiang Program (2013) under grant No. 13PJ1400500. J.Z. acknowledges the support by the program for New Century Excellent Talents in Universities grant No. NCET-13-0431.

■ REFERENCES

(1) Rowe, D. M. *Thermoelectrics Handbook: Macro to Nano*, 1st ed; CRC Press, Taylor & Francis Group: Boca Raton, FL, 2006.

(2) MacDonald, D. K. C. *Thermoelectricity: An Introduction to the Principles*, 1st ed; Dover Publications: New York, 2006.

(3) Zhao, L.-D.; He, J.; Berardan, D.; Lin, Y.; Li, J.-F.; Nanc, C.-W.; Dragoe, N. BiCuSeO Oxyselenides: New Promising Thermoelectric Materials. *Energy Environ. Sci.* **2014**, *7*, 2900−2924.

(4) Zebarjadi, M.; Esfarjani, K.; Dresselhaus, M. S.; Ren, Z. F.; Chen, G. Perspectives on Thermoelectrics: From Fundamentals to Device Applications. *Energy Environ. Sci.* **2012**, *5*, 5147−5162.

(5) Vineis, C. J.; Shakouri, A.; Majumdar, A.; Kanatzidis, M. G. Nanostructured Thermoelectrics: Big Efficiency Gains from Small Features. *Adv. Mater.* **2010**, *22*, 3970−3980.

(6) Yee, S. K.; LeBlanc, S.; Goodson, K. E.; Dames, C. $ per W Metrics for Thermoelectric Power Generation: Beyond ZT. *Energy Environ. Sci.* **2013**, *6*, 2561−2571.

(7) Poudel, B.; Hao, Q.; Ma, Y.; Lan, Y.; Minnich, A.; Yu, B.; Yan, X.; Wang, D.; Muto, A.; Vashaee, D.; Chen, X.; Liu, L.; Dresselhaus, M. S.; Chen, G.; Ren, Z. High-Thermoelectric Performance of Nanostructured Bismuth Antimony Telluride Bulk Alloys. *Science* **2008**, *320*, 634−638.

(8) Hsu, K. F.; Loo, S.; Guo, F.; Chen, W.; Dyck, J. S.; Uher, C.; Hogan, T.; Polychroniadis, E. K.; Kanatzidis, M. G. Cubic $AgPb_mSbTe^{2+}{}_m$: Bulk Thermoelectric Materials with High Figure of Merit. *Science* **2004**, *303*, 818−821.

(9) Vining, C. B.; Laskow, W.; Hanson, J. O.; Van der Beck, R. R.; Gorsuch, P. D. Thermoelectric Properties of Pressure-Sintered $Si_{0.8}Ge_{0.2}$ Thermoelectric Alloys. *J. Appl. Phys.* **1991**, *69*, 4333−4340.

(10) Snyder, G. J.; Toberer, E. S. Complex Thermoelectric Materials. *Nat. Mater.* **2008**, *7*, 105−114.

(11) Nam, W. H.; Lim, Y. S.; Choi, S.-M.; Seo, W.-S.; Lee, J. Y. High-Temperature Charge Transport and Thermoelectric Properties of A Degenerately Al-Doped ZnO Nanocomposite. *J. Mater. Chem.* **2012**, *22*, 14633−14638.

(12) Jung, K. H.; Lee, K. H.; Seo, W. S.; Choi, S. M. An Enhancement of a Thermoelectric Power Factor in a Ga-Doped ZnO System: A Chemical Compression by Enlarged Ga Solubility. *Appl. Phys. Lett.* **2012**, *100*, 253902.

(13) Qu, X.; Wang, W.; Lv, S.; Jia, D. Thermoelectric Properties and Electronic Structure of Al-Doped ZnO. *Solid State Commun.* **2011**, *151*, 332−336.

(14) Tsubota, T.; Ohtaki, M.; Eguchi, K.; Arai, H. Thermoelectric Properties of Al-Doped ZnO as a Promising Oxide Material for High-Temperature Thermoelectric Conversion. *J. Mater. Chem.* **1997**, *7*, 85−90.

(15) Isobe, S.; Tani, T.; Masuda, Y.; Seo, W. S.; Koumoto, K. Thermoelectric Performance of Yttrium-Substituted $(ZnO)_5In_2O_3$ Improved through Ceramic Texturing. *Jpn. J. Appl. Phys.* **2002**, *141*, 731.

(16) Jood, P.; Mehta, R. J.; Zhang, Y.; Peleckis, G.; Wang, X.; Siegel, R. W.; Borca-Tasciuc, T.; Dou, S. X.; Ramanath, G. Al-Doped Zinc Oxide Nanocomposites with Enhanced Thermoelectric Properties. *Nano Lett.* **2011**, *11*, 4337−4342.

(17) Ohtaki, M.; Araki, K.; Yamamoto, K. High Thermoelectric Performance of Dually Doped ZnO Ceramics. *J. Electr. Mater.* **2009**, *38*, 1234−1238.

(18) Chen, Y.; Zhao, Y.; Liang, Z. Solution Processed Organic Thermoelectrics: Towards Flexible Thermoelectric Modules. *Energy Environ. Sci.* **2015**, DOI: 10.1039/C4EE03297G.

(19) He, M.; Qiu, F.; Lin, Z. Towards High-Performance Polymer-Based Thermoelectric Materials. *Energy Environ. Sci.* **2013**, *6*, 1352−1361.

(20) Du, Y.; Shen, S. Z.; Cai, K.; Casey, P. S. Research Progress on Polymer-Inorganic Thermoelectric Nanocomposite Materials. *Prog. Polym. Sci.* **2012**, *37*, 820−841.

(21) Wu, Z. H.; Xie, H. Q.; Zhai, Y. B. Enhanced Thermoelectric Figure of Merit in Nanostructured ZnO by Nanojunction Effect. *Appl. Phys. Lett.* **2013**, *103*, 243901.

(22) Novoselov, K. S.; Geim, A. K.; Morozov, S. V.; Jiang, D.; Zhang, Y.; Dubonos, S. V.; Grigorieva, I. V.; Firsov, A. A. Electric Field Effect in Atomically Thin Carbon Films. *Science* **2004**, *306*, 666−669.

(23) Thiyagarajan, P.; Oh, M.-W.; Yoon, J.-C.; Jang, J.-H. Thermoelectric Properties of Nanoporous Three-Dimensional Graphene Networks. *Appl. Phys. Lett.* **2014**, *105*, 033905.

(24) Xiao, N.; Dong, X.; Song, L.; Liu, D.; Tay, Y.; Wu, S.; Li, L.-J.; Zhao, Y.; Yu, T.; Zhang, H.; Huang, W.; Hng, H. H.; Ajayan, P. M.; Yan, Q. Enhanced Thermopower of Graphene Films with Oxygen Plasma Treatment. *ACS Nano* **2011**, *5*, 2749−2755.

(25) Ni, X.; Liang, G.; Wang, J.-S.; Li, B. Disorder Enhances Thermoelectric Figure of Merit in Armchair Graphane Nanoribbons. *Appl. Phys. Lett.* **2012**, *95*, 192114.

(26) Dong, J.; Liu, W.; Li, H.; Su, X.; Tang, X.; Uher, C. In Situ Synthesis and Thermoelectric Properties of PbTe-Graphene Nanocomposites by Utilizing A Facile and Novel Wet Chemical Method. *J. Mater. Chem. A* **2013**, *1*, 12503−12511.

(27) Zhao, Y.; Dyck, J. S.; Burda, C. Toward High-Performance Nanostructured Thermoelectric Materials: The Progress of Bottom-up Solution Chemistry Approaches. *J. Mater. Chem.* **2011**, *21*, 17049−17058.

DOI: 10.1021/am507882f
ACS Appl. Mater. Interfaces 2015, 7, 3224−3230

(28) Nam, W. H.; Kim, B. B.; Seo, S. G.; Lim, Y. S.; Kim, J.-Y.; Seo, W.-S.; Choi, W. K.; Park, H.-H.; Lee, J. Y. Structurally Nanocrystalline-Electrically Single Crystalline ZnO-Reduced Graphene Oxide Composites. *Nano Lett.* **2014**, *14*, 5104−5109.
(29) Lundstrom, M. *Fundamentals of Carrier Transport*, 2nd ed; Cambridge University Press: Cambridge, U.K., 2000.
(30) Aschroft, N. W.; Mermin, N. D. *Solid State Physics*, 1st ed; Harcout College Publishers: Orlando, FL, 1976.
(31) Zhou, J.; Li, X.; Chen, G.; Yang, R. Semiclassical Model for Thermoelectric Transport in Nanocomposites. *Phys. Rev. B* **2010**, *82*, 115308.
(32) Nag, B. R. *Electron Transport in Compound Semiconductors*; Springer-Verlag: Berlin, Germany, 1980.
(33) Minnich, A.; Chen, G. Modified Effective Medium Formulation for the Thermal Conductivity of Nanocomposites. *Appl. Phys. Lett.* **2007**, *91*, 073105.

DOI: 10.1021/am507882f
ACS Appl. Mater. Interfaces 2015, 7, 3224−3230